



Improving soil heat and moisture forecasting for arid and semi-arid regions: A comparative study of four mathematical algorithms

Junjun Yang^a, Jianmin Feng^a, and Zhibin He^b

^aCollege of Resource & Environment and Historical Culture, Xianyang Normal University, Xianyang, China; ^bKey Laboratory of Ecohydrology of Inland River Basin, Linze Inland River Basin Research Station, Chinese Ecosystem Research Network, Northwest Institute of Eco-Environment and Resources, Chinese Academy of Sciences, Lanzhou, China

ABSTRACT

Mathematical modeling is extensively used for ecohydrological processes because it facilitates data acquisition. However, modeling of soil moisture and heat remains challenging in dry ecosystems. In this study, we examined the performance of four models in simulating hydrological processes in a semi-arid mountain grassland (SMG), and in shrubland forming a transitional zone between the desert and an oasis (desert–oasis ecotone; DOE) in northwestern China. We used precipitation, air temperature, humidity, atmospheric pressure, and other meteorological variables to estimate moisture and temperature at different soil depths. Four methods were used to test model performance, including partial least squares (PLS) regression, stepwise multiple linear regression (SMR), back-propagation artificial neural network (BPANN), and neural network time series. Our results showed that BPANN had the best prediction accuracy and supplied a robust modeling framework capable of capturing nonlinear environmental processes by improving the stability of the weight-learning process. Soil depth in SMG for which model performance was optimized was 20 cm for PLS and SMR. Additionally, artificial neural networks (ANNs) have a remarkable applicability compared to other algorithms for increased accuracy in time-series predictions; however, they could not depict soil moisture or temperature dynamics at 160 cm depth in SMG, and at 10 cm depth in DOE. Using conventional meteorological data as primary predictors, and avoiding the complexity of distributed hydrological models can be helpful in developing a regional capacity for soil moisture and heat forecasting.

ARTICLE HISTORY



Received 20 January 2017
Accepted 20 November 2017

KEYWORDS

Artificial neural network;
mathematical algorithm;
partial least squares
regression; semi-arid

Introduction

Soil moisture and temperature dynamics influence calculations of water and energy budgets, and water circulation on Earth, and are critical to research on global climate change (Wofsy et al. 1993; Kokaly and Clark 1999; Klemas, Finkl, and Kabbara 2014). Arid ecosystems in China are under intense development and climate change pressure that lead to increasing land degradation. To reverse land degradation, vegetation restoration programs are growing in popularity. However, the efficacy of these programs in arid

CONTACT Junjun Yang  junjun_yang@126.com  College of Resource & Environment and Historical Culture, Xianyang Normal University, Xianyang 712000, China.

Color versions of one or more of the figures in the article can be found online at www.tandfonline.com/uasr.

© 2017 Taylor & Francis

ecosystems is entirely dependent on water resources management, including estimating of groundwater budgets, management of agricultural irrigation, and monitoring of drought conditions (Dumedah, Walker, and Chik 2014; Yang et al. 2016), among others. Therefore, a high level of precision in soil moisture monitoring is critical to these operations.

Soil temperature at a soil-layer resolution is an indicator of the thermal properties of the soil profile; it has fundamental uses in climatology, engineering, and agriculture, and plays an essential role in numerical hydrological modeling (Gao et al. 2008) and in agricultural management (Yilmaz et al. 2009).

Drought conditions remain relatively under-studied compared to other aspects of the water cycle (Thomas, Qin, and Gian-Kasper 2013). The process of drought formation is complex and unpredictable due to the inherent nonlinear relationships between meteorological factors and topographic parameters. Additionally, increases in global temperature threaten the modest water resources of arid lands, as higher temperatures not only increase evaporation rates, but also plant water demand (Hutchinson and Herrmann 2008). Furthermore, due to low water retention and high infiltration and leaching rates, sandy soils are generally dry and therefore not suitable for plant growth.

Predictions of soil moisture may involve complex modeling such as possible with ecohydrological models, or simple forecasting. Unlike ecohydrological models, soil moisture-forecasting systems do not incorporate meteorological factors or explicit mechanisms driving soil moisture. For that reason, data-driven models such as stepwise multiple linear regression (SMR) and artificial neural networks (ANNs) have gained in popularity in recent years (Dursun and Ozden 2014; Ganguli and Reddy 2014; Nourani et al. 2014). Data-driven models use programming with statistical and machine-learning approaches to solve applied problems. For example, the ANN algorithm could achieve high accuracy in estimating missing soil moisture records. This is possible because ANN is a regression-based dynamic network that allows feedback connections through discrete-time estimation (Dumedah, Walker, and Chik 2014). Ganguli and Reddy (2014) used a support-vector machine-copula approach to show that it can improve drought-forecasting capability. Yu et al. (2012) used *in-situ* surface-air temperature, solar radiation, relative humidity, and antecedent soil temperature and moisture to predict soil moisture at multiple layers using support-vector machines and data-assimilation techniques. This research indicated that data-driven techniques can be used for soil moisture forecasting. Nourani et al. (2014) reviewed the hybrid wavelet and artificial intelligence (AI)-based models for functionality in simulating hydrologic processes, and concluded that the robustness and accuracy of wavelet-AI justified the increased use of this approach in hydrology.

In practical situations, the main focus is on providing accurate forecasting for selected areas, and the usefulness of a model depends on its simplicity and robustness in solving actual problems (Latt and Wittenberg 2014). A recent review of the applications of data-driven models in hydrological processes revealed that almost all of the existing studies concentrated on areas with multiple rainfalls. However, soil moisture is exceedingly low in arid and semi-arid regions; therefore, simulations or estimations of soil moisture dynamics are challenging (Si et al. 2015), and it is not clear whether nonlinear data-driven models can provide a satisfactory performance in such conditions.

The relationships among soil moisture conditions, vegetation succession, and ecosystem restoration and agriculture management are complex, and they require a hybrid model with multi-step forecasting for both regression models and ANN (Latt and

Wittenberg 2014). This approach was applied to the Chindwin River Basin in northern Myanmar, an area with a tropical monsoon climate, and the conclusions were not applicable for arid regions (He et al. 2014). Ma et al. (2004) found that soil moisture correlated with environmental factors at different scales in areas where annual precipitation was between 500 and 850 mm; they used this correlation to calculate thresholds of soil moisture specific for meadows, shrubs, and forests. Si et al. (2015) analyzed the performance of an adaptive neuro-fuzzy technique in soil moisture modeling using antecedent moisture conditions at 40 and 60 cm soil depths in an extremely arid area of the Ejina basin, in the lower reaches of the Heihe River in China. However, the investigation did not account for the superficial soil layer at 0–10 cm, which is extremely sensitive to weather conditions, or the deepest soil layer at >100 cm, where soil moisture affects deep roots, important for plant survival (Breshears and Barnes 1999). Despite the efforts at modeling of soil hydrology, there are still no tools that can efficiently predict soil moisture and heat in arid areas.

The work reported here had three aims: (1) to verify the feasibility of simulating soil water content and heat in arid regions using weather parameters; to achieve this, we compared four mathematical algorithms for modeling complex water and heat transmission systems, (2) to determine which model performed best; here, we evaluated the response to climate factors of soil water and heating processes at different soil depths. Our results provide a reference for vegetation restoration and agricultural management. Vegetation restoration in mountainous areas in the desert–oasis ecotone (DOE) is critical to the recovery of regional ecological function. Accurate estimation of water and heat transmission in the soil profile is vital to an effective design of vegetation restoration, and in farm management. This study was an effort to improve soil moisture and heat forecasting.

Methodology

Study sites

Soil moisture and temperature data were obtained at two locations: a grassland bordering a *Picea crassifolia* Kom. forest in the Qilian Mountains, and a desert–oasis transition zone in Linze County, both sites near the town of Zhangye, Gansu Province, China (Figure 1).

Semi-arid mountain grassland

The first site was a semi-arid mountain grassland (SMG) in the Pailugou catchment in the Qilian Mountains, northwestern China (38°33′17″N, 100°17′9″E). This is a shady forest land at an elevation of 2700 m, with a mean slope of about 20°, mean annual precipitation of 375.5 mm, and average temperature of 0.5°C; data used here were means of the past 15 years (He et al. 2012). Vegetation reaches about 25 cm in height, with mean plant cover of about 90% (He et al. 2012; Yang et al. 2016). Soils are mainly montane chestnut, found primarily in sunny exposures at elevations of 2720–3000 m. Mean soil depth is about 40 cm, with organic matter content of the surface soil of 2–4%, and pH of 8.0–8.5. Additionally, mountain forest grey-brown soils, found on shaded slopes at elevations between 2600 and 3770 m (Yang et al. 2016), reach almost 67 cm in depth, and exhibit a 20–30 cm depth of sod; percentage of clay, silt, and sand is 14.2, 30, and 55.8, respectively; these soils exhibit a pH value of 7.0–8.0, and an organic matter content in the upper soil of

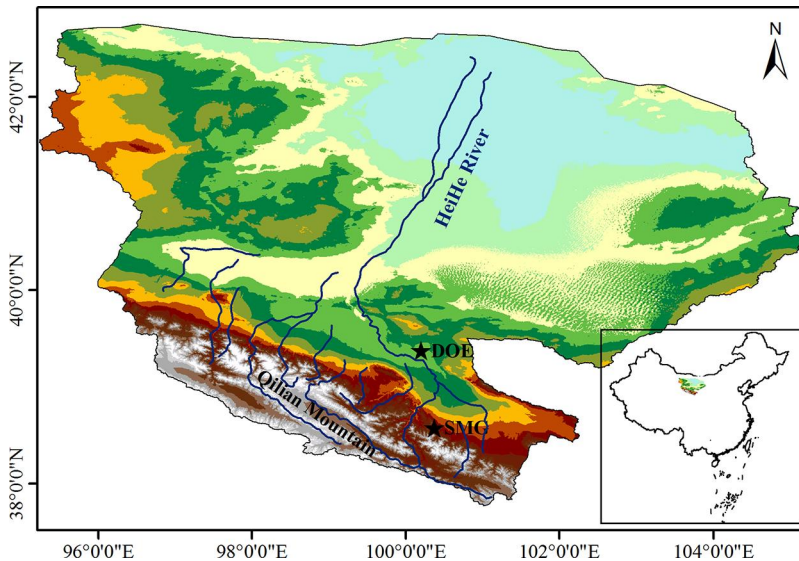


Figure 1. Map showing study locations semi-arid mountain grassland (SMG) and desert–oasis ecotone (DOE). (Note: The background picture is Shuttle Radar Topography Mission DEM of the Heihe River Basin, the peak elevation is at the Qilian Mountain (elevation = 5328 m), and the lowest point is at the Alashan Highland end of the Heihe River in the north (elevation = 852 m)).

about 10–25%. Vegetation on the northern (shaded), northwestern, and northeastern (partly shaded) slopes includes native grasslands and *P. crassifolia* Kom. plantation forests. The southern, southwestern, and southeastern exposures (sunny and partly sunny) are dominated by low grasses. The study site is near the timberline. Statistical characterization of soil temperature and moisture for both sites is found in Table 1.

Desert–oasis ecotone

The second site was located at the northeastern edge of the Zhangye oasis in northwestern China (39°22'9"N, 100°07'2"E) at an elevation of 1382 m, and near the Linze Ecological Observational and Experimental Station. Topography is characteristic of a vast plain. It is a semi-desert transitional zone between oasis and desert, characterized by sparse vegetation and a sandy substrate. The zonal soil is desert soil, with coarse texture (particle size between 0.05 and 0.25 mm in diameter account for 80–90% of the total). The climate is continental arid temperate. Mean annual precipitation is 117 mm (Zhao, Li, and Fang 2007), falling mainly in summer, with the dryness index (evaporation divided by

Table 1. Daily soil water content and temperature in the 0–20 cm layer at SMG (statistical values for years from 2009 to 2013) and DOE (for years from 2010 to 2011).

Site	Parameter	Number of records	Range	Minimum	Maximum	Mean	Std. error	Std. deviation	Variance
SMG	Soil water content	680	32.68	7.5	40.18	18.16	0.33	8.68	75.26
	Soil temperature	680	26.08	−12.53	13.55	1.15	0.26	6.74	45.38
DOE	Soil water content	394	9.55	1.66	11.21	3.68	0.12	2.34	5.46
	Soil temperature	394	35.55	−3.79	31.76	20.85	0.43	8.51	72.5

SMG, semi-arid mountain grassland; DOE, desert–oasis ecotone.

precipitation) of 20.54. Air temperature averaged about 7.6°C between the years 1965 and 2000 (Zhao, Li, and Fang 2007). The dominant species are shrubs *Nitraria sphaerocarpa* Maxim and Chenopodiaceae. Soil texture is dominated by wind-blown sand. Mean soil moisture was about 2.13% at the 0–20 cm soil depth (He and Zhao 2004), and 3.4% at 10–20 cm depth. Vegetation cover (desert shrubs) ranges from 5 to 7% and the landscape is dominated by fixed, semi-fixed, semi-mobile, and mobile sand dunes (Zhao and Liu 2010).

Data

Data were collected in 2009 and 2013 at SMG and in 2010 and 2011 at DOE. Time periods of the observations varied. Observations at SMG included a training period from 20 January 2010 to 31 December 2010 and validation period from 1 January 2011 to 30 November 2011. Observations at DOE included a modeling period from 1 February 2013 to 30 September 2013 and validation period from 17 May 2009 to 15 October 2009. We collected data on soil moisture with a time domain reflectometer (Campbell Scientific, Inc., Logan, Utah). Moisture probes were placed horizontally in the middle of each of the tested soil depths. Soil water content for all soil depths at both study sites was volumetric. Soil temperature data were collected continuously with Campbell 109ss temperature sensor probes (Campbell Scientific, Inc., Logan, Utah), and had the same time series as soil moisture data. Depth of monitoring was the same for both types of probes at 10, 20, 30, 40, 50, 60, 80, and 100 cm. The type of meteorological data obtained from an automatic comprehensive weather station, soil depth, and type of meteorological data used in the study are given in Table 2.

All data were collected at 30-min intervals and averaged to daily values for this study. Data were processed, and numerical simulations were performed using Matlab R2010b (The Mathworks, Inc., Natick, MA).

Input variables for the models were a combination of meteorological factors, and the calibration and validation data consisting of soil moisture or soil temperature vector at each soil depth. All models were constructed using the same input variables and simulation periods.

Table 2. Soil characteristics at two study sites for individual soil depths.

Depth		Meteorological parameters	
SMG (cm)	DOE (cm)	SMG	DOE
20	10	Temperature max. 1.5 m (°C)	Temperature mean 1.5 m (°C)
40	20	Temperature min. 1.5 m (°C)	Land surface temperature (°C)
60	30	Temperature mean 1.5 m (°C)	Humidity 1.5 m (%)
80	40	Land surface temperature (°C)	Global radiation (W/m ²)
120	50	Humidity 1.5 (%)	Atmospheric pressure (Pa)
160	60	Net radiation (W/m ²)	Wind speed (m/s)
	80	Global radiation (W/m ²)	Precipitation (mm)
	100	Reflection	
		Atmospheric pressure (Pa)	
		Wind speed (m/s)	
		Heat flux (W/m ²)	
		Precipitation (mm)	

SMG, semi-arid mountain grassland; DOE, desert–oasis ecotone.

Note: Height of measurement for atmospheric pressure was 0.5 m, precipitation was 1.0 m, and other meteorological parameter was 1.5 m at both study sites.

Models used in forecasting

In this study, four algorithms were compiled with Matlab script, and the operational processes of all algorithms were similar to each other. We describe the details of PLS's running processes as an example of any one algorithm. First, we compiled the PLS function in a functional form, which was used in calling of the function. Second, we compared meteorological variables (often called independent X) with the validation data (often called dependent Y ; our variables were soil water content or soil temperature at different soil depths). All the input and validation variables were combined as one-time input data. In the third step, we combined the independent variables with their sensitivities to predict values for the dependent variables. Last, validation and the evaluation indicators were produced as separate files. The concept, characteristics, and arithmetic of the four algorithms are shown below.

Partial least squares regression

The partial least squares (PLS) regression is a statistical method that generalizes and combines features from principal component regression and multiple regression (PLSR) (Mevik and Wehrens 2007). A PLS attempts to determine a multidimensional direction in X space that explains the maximum multidimensional variable direction in Y space, where X and Y are two matrices. PLS is particularly suited for situations when multicollinearity occurs among input variables, and standard regression fails (unless it is controlled); steps of the algorithm can be found in Abdi (2007).

Stepwise multiple linear regression

Stepwise multiple linear regression is the extended form of simple linear regression. SMR aims to intercept as much of the variability of a response as possible, leaving as little of the variation as possible to be explained as "noise" (Kokaly and Clark 1999). The general form for n independent variables can be expressed as:

$$Y = \alpha_0 + \alpha_1 X_1 + \alpha_2 X_2 + \dots + \alpha_n X_n + \varepsilon \quad (1)$$

where Y is the response variable; α_0 , α_1 , α_2 , and α_n are regression coefficients; ε is error; and X_1 , X_2 , and X_n are independent variables.

Partial least squares and SMR determined the strength of the linear relationships between the input and output variables. We chose SMR because it eliminated the influence of strong correlations among meteorological variables (e.g., air temperature, net radiation, and wind speed).

Back-propagation artificial neural network

A neuron is a nonlinear, parameterized, and bounded function that is fundamental to the operation of a neural network (Dreyfus 2005). A neural network is a parallel-distributed processor composed of simple processing units, with a natural propensity for storing experiential knowledge and making it available for use (Haykin 1999). A neural network may be thought of as self-evolving approach. Back-propagation, developed by Rumelhart, Hinton, and Williams (1986), is a gradient-descent algorithm that compares simulated outputs with observed values to minimize error; it has been widely used since its development. Computation in each unit is accomplished in two steps. The first step involves a *summation junction*, a linear function that computes the weighted-sum of the

inputs. The second step engages *nonlinear activation*, which returns the final transformed value of the weighted sum. Figure 2 shows an example of a multi-layered back-propagation artificial neural network (BPANN) that can be used to associate input consisting of three units with two decisions.

In Figure 2, net and H can be represented as [Eq. (2)] and [Eq. (3)].

$$\text{net}_{1h} = \sum_i W_{ih} \times X_i - \theta_{1h} \quad (2)$$

$$H_{1h} = f(\text{net}_{1h}) = \frac{1}{1 + e^{-\text{net}_{1h}}} \quad (3)$$

where W is the weight between neurons (such as W_{nm} in Figure 2), X_i is the i th input predictor variable (such as X_n in Figure 2), h is the number of transfer functions (activation functions that define output of that node given input, such as the number of transfer functions of hidden layer 1 in Figure 2) for the hidden layer 1, θ is a transfer function (such as θ_{1h} of hidden layer 1 in Figure 2). The network shown is well connected, and a neuron (a combination of net_{mh} and H_{mh} in Figure 2) at any one layer of the network can be linked to any nodes (any one of the input variables, neurons or the output variables, such as X_n , H_{1h} or Y_2 in Figure 2) in any other layers. Signals propagate through the network in two directions, with the function signal (weight that varies as learning proceeds, such as W_{nm} in

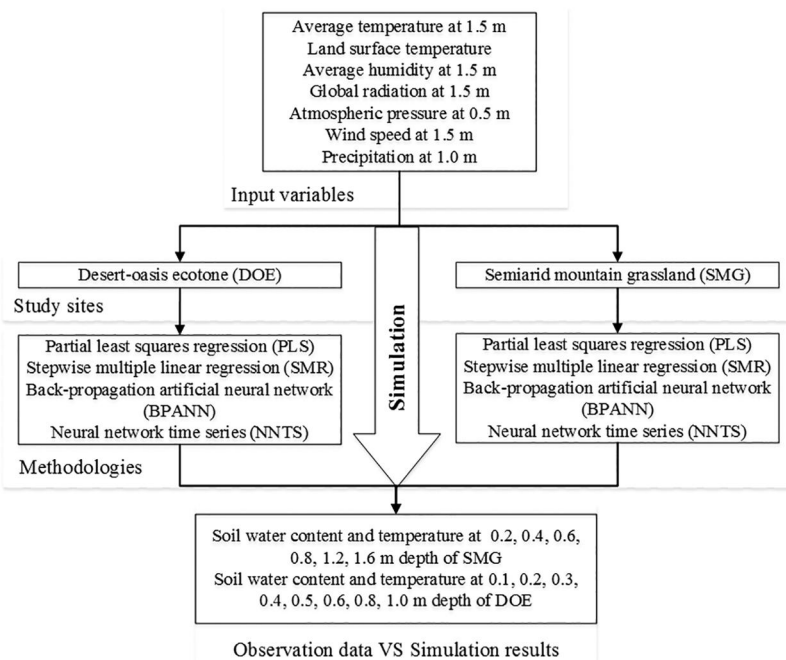


Figure 2. Diagram of a multi-layered BPANN with hidden layers and back-propagation of error signals. *Notes:* hidden layer is a system of weighted “connections,” which connect via the “input layer” link to an “output layer”; ellipses indicate variables used in BPANN, x_1, x_2, \dots, x_n indicate neurons, $\text{net}_{11} \dots \text{net}_{1h}$ indicate nodes of the network, rectangles are components of BPANN network, arrows indicate explanations of the elements used in BPANN network, triangle indicates evaluation index of the network, grey background indicates that the content explains the construction of BPANN network. *Note:* BPANN, back-propagation artificial neural network.

Figure 2) moving forward, and the error signal moving backward. A function signal enters the network at the input terminal, and travels to the output. Similarly, an error signal produced at the output terminal travels backward through the network layers (Figure 2).

Hidden neurons (neurons that cannot be controlled by researchers in the computational processes) involve two computations. First computation generates the function signal, represented as a continuous nonlinear function of the input signal and of the synaptic weights (w_{ij}) associated with the neuron. Second is the computation of an estimate of the gradient vector (the derivative of the loss function with each term w_{nm} to \bar{w} , where \bar{w} is the mean of the weights) needed for the backward pass through the network.

The error signal (output) of a neuron i for an iteration n may be described as:

$$e_i(n) = d_i(n) - y_i(n) \quad (4)$$

where $d_i(n)$ is the observed value, and $y_i(n)$ is the modeled value. Then, the total error $\varepsilon(n)$ is calculated as the sum of errors $1/2e_i^2(n)$ over all neurons.

$$\varepsilon(n) = \frac{1}{2} \sum_{i=C} e_i^2(n) \quad (5)$$

If N is set equal to the total number of configurations (one configuration is a combination of the input variable, hidden layer, and output variable) present in the training set, the average squared total error is the sum $\varepsilon(n)$ over all n normalized for the set size N . Thus, it may be represented as:

$$\varepsilon_{av} = \frac{1}{N} \sum_{n=1}^N \varepsilon(n) \quad (6)$$

Because neural networks do not require that input data satisfy specific statistical distributions, a distinctive benefit of using neural networks is the opportunity to work with multiple sources of data (Brown et al. 2008).

During the training of ANN, the modeler must confirm that some parameters increase the accuracy and convergence speed of ANN; this concerns such parameters as the number of hidden layers and neurons in each layer. Because there is no general and explicit method for the selection of optimal parameters for ANN, we used an automated trial and error method. In the first step, we determined the performance criteria of ANN. In our study, four criteria were considered: coefficient of determination (R^2), root mean square error, the mean absolute relative error, and relative percent deviation (D_{RP}). Definition and description of each criterion can be found below. We determined the number of neurons in the layers in the second step, and the desirability function (a function used to get optimal values of input variables) used to optimize responses simultaneously, in the third step. For analysis of performance for a combination of effective parameters, we used a genetic algorithm (GA) applied to finding the optimum combination of sets of factors. For more on GA, see Koza (1992) and Ahn (2006).

Neural network time series

The neural network time series (NNTS) fits the data with a two-layer feed-forward network (an ANN in which information moves in only one direction), a linear transfer function in the output layer, and a sigmoidal transfer function in the hidden layer (Frank, Davey, and Hunt 2001). Differences between NNTS and BPANN exist if there is a back-propagation

signal and a time-series function in BPANN. The delay in the artificial network was set for 2 days, and the hidden layer size was 12. Because neural networks can be viewed as highly nonlinear functions, the training processes may be considered as function optimization; here, three optimization algorithms were used, including Levenberg–Marquardt (*trainlm*), Bayesian regularization (*trainbr*), and scaled conjugate gradient (*trainscg*) to determine the best network parameters, including weights and biases in network learning. For our application, we used the default training function (*trainlm*) because the output was obtainable during network training. We used the open-loop architecture with true output instead of the estimated output; this way, we obtained a more efficient algorithm for training. The default number of hidden neurons was set to 10, and the default number of delays was 2.

The network uses tapped delay lines to stockpile previous values of the $x(t)$ and $y(t)$ sequences (a list of observational series or validation series with time order), these can be used to solve time-series problems. There are two input factors, input series $x(t)$ and an output series $y(t)$. For this study, we wanted to predict the values of $y(t)$ (e.g., soil moisture) from previous values of $x(t)$ (e.g., precipitation), with no knowledge of previous values of $y(t)$. This mapping relationship between input and output data can be written as follows:

$$y(t) = f((y(t-1), \dots, y(t-d))) \quad (7)$$

where t is the number of days to simulation, and d is the number of delay days. The algorithm uses error-autocorrelation and input-error cross-correlation functions to verify network performance. For a high-performing prediction model, the value of the error-autocorrelation function cannot equal 0 at 0 lag, which means that the prediction errors must be completely uncorrelated with each other. In case of a significant correlation in the prediction error, network retraining (changing the initial weights and biases of the network) or increasing the number of delays in the tapped delay lines (a delay line with at least one “tap”) may improve prediction performance.

When network performance is unsatisfactory during validation, it is possible to (1) train it once more, (2) increase the number of neurons and/or the number of delays, and (3) obtain a larger training data set. Over-fitting of the training can occur when validation performance decreases further, but the training set is of high quality; in such case, the number of neurons can be reduced to improve results.

The advantages and disadvantages of the four numerical models are summarized in Table 3.

Assessment of model performance

Standard statistical criteria facilitate model evaluation for accuracy of simulation results and of measured records (Latt and Wittenberg 2014). We used coefficient of determination (R^2) [Eq. (8)], error sum of squares (E_{RMS}) [Eq. (9)], mean absolute error (E_{MA}) [Eq. (10)], and the ratio of standard deviation to E_{RMS} (D_{RP}) [Eq. (11)]; D_S [Eq. (12)] is an intermediate variable between Eqs. (10) and (11). It is very helpful to confirm the strength of various approaches, and we considered D_{RP} in our uncertainty estimation.

$$R^2 = 1 - \frac{\sum_{i=1}^n (W_s - W_f)^2}{\sum_{i=1}^n (W_s - \overline{W_s})^2} \quad (8)$$

Table 3. A comparison of advantages and disadvantages of the four algorithms.

Algorithm name	Characteristics	Advantages	Disadvantages
PLS	Useful in common cases where the number of descriptors (independent variables) is comparable to or greater than the number of data points, and/or other factors exist leading to correlations between variables	Robust; non-orthogonal descriptors; multiple biologic results; much lower risk of chance correlation	Higher risk of overlooking “real” correlations; sensitivity to the relative scaling of the descriptor
SMR	The dependent variable must be continuous or nearly continuous, the independent variable can be categorical or continuous	Better prediction from multiple predictors; can “avoid” picking/depending on a single predictor; can “avoid” non-optimal combinations of predictors	Stepwise methods will not necessarily produce the best model if there are redundant predictors; stepwise methods have an inflated risk of capitalizing on chance features of the data
BPANN	BPANN can be used to perform nonlinear statistical modeling, and provides a new alternative to logistic regression	Requires less formal statistical training; ability to implicitly detect complex nonlinear relationships between dependent and independent variables; ability to detect all possible interactions between predictor variables; availability of multiple training algorithms	“Black box” nature; greater computational burden; prone to over-fitting; the empirical nature of model development
NNTS	Fits the data with a two-layer feed-forward network, a linear transfer function in the output layer, and a sigmoidal transfer function in the hidden layer	Has a time-series function; can approximate nonlinear functions without any <i>a priori</i> information about the properties of data series	There is no “perfect” machine-learning method; the Vapnik–Chervonenkis (VC) dimension of neural networks is unclear; neural networks cannot be retrained

PLS, partial least squares regression; SMR, stepwise multiple linear regression; BPANN, back-propagation artificial neural network; NNTS, neural network time series.

Note: Vapnik–Chervonenkis (VC) is a form of computational learning theory, which attempts to explain the neural network learning processes from a statistical point of view.

$$E_{\text{RMS}} = \sqrt{\frac{\sum_{i=1}^n (W_o - W_s)^2}{n}} \quad (9)$$

$$E_{\text{MA}} = \frac{\sum_{i=1}^n \left| \frac{W_s - W_f}{W_s} \right|}{n} \quad (10)$$

$$D_{\text{RP}} = \frac{D_s}{E_{\text{RMS}}} \quad (11)$$

$$D_s = \sqrt{\frac{\sum_{i=1}^n (W_s - \overline{W_s})^2}{n - 1}} \quad (12)$$

where W_o is the time series of measurement values (soil moisture or soil temperature), W_f is the observation fitted with a linear function, W_s is the value predicted from measurement data, $\overline{W_s}$ is a series of mean predicted values, i is the number of samples, n is the number of

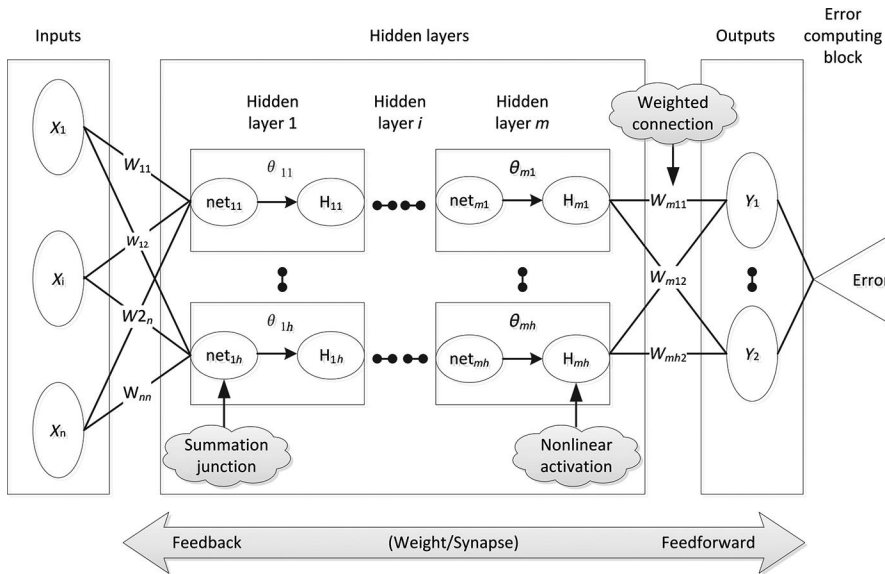


Figure 3. Input variables and methodologies of simulation processes.

days with computed parameters. Low values of E_{RMS} and E_{MA} indicate a better fit, with a value of 0 indicating optimal model performance. R^2 is the correlation coefficient between the observed and the predicted values, with a range from 0 to 1.

According to Chang et al. (2001), D_{RP} can be categorized into three types: A ($D_{RP} \geq 3.0$), B ($2 < D_{RP} < 3.0$), and C ($D_{RP} \leq 2.0$). A indicates that models perform well, B indicates that models perform in general and can be improved with calibration strategies, and C meaning that variables cannot be predicted reliably using a model correction, and the model cannot be used for forecasting (Fontaine, Schirmer, and Horr 2002). We used these criteria to determine model performance.

Figure 3 shows the flow between input parameters, numerical algorithms, study sites, and simulation output data.

Results

Least squares regression and stepwise multiple linear regression

Both statistical and graphical model results were evaluated. The performance of PLS and SMR was poor for both model calibration and validation, except for the PSL validation results for soil temperature at DOE (Table 4 and Figure 4). These results indicated that the two models (PLS and SMR) could not simulate the feedback relationships between meteorological factors and soil water and heat transmission processes. However, the linear functions can be used for the soil-temperature simulation at DOE. If we excluded the calibration period and attended to the validation results, the performance at 20 cm depth at SMG was acceptable; at other depths, performance was still poor ($D_{RP} < 2.0$), with the performance rating of "C."

Table 4. Ratio of standard deviation to error sum of squares (D_{RP}) for different soil depths at SMG and DOE following model evaluation between the calibration and validation, CSM: Calibration of soil moisture, CST: Calibration of soil temperature, and VSM and VST: Validation of soil moisture and temperature.

	Soil depth (cm)	SMG				Soil depth (cm)	DOE			
		PLS	SMR	BPANN	NNTS		PLS	SMR	BPANN	NNTS
CSM	20	1.00	0.97	18.26	18.92	10	0.94	0.80	2.29	2.67
	40	1.26	1.67	52.67	52.47	20	1.05	1.05	7.20	11.66
	60	1.92	1.92	76.02	81.65	30	0.63	0.81	28.12	4.57
	80	1.06	1.29	13.65	14.26	40	0.79	0.87	25.85	17.22
	120	1.12	1.48	58.12	39.92	50	1.42	1.43	38.26	27.49
	160	1.28	1.35	30.64	32.90	60	2.35	2.40	37.79	25.00
CST						80	3.18	3.57	53.69	31.72
	20	6.66	6.59	22.35	19.79	100	3.31	3.63	52.36	34.98
	40	3.48	16.81	58.72	47.04	10	4.16	4.37	12.73	12.76
	60	2.57	6.89	95.45	89.96	20	3.72	4.42	28.32	21.60
	80	2.02	3.97	119.47	130.83	30	3.20	4.21	27.74	30.43
	120	1.39	2.12	101.80	87.62	40	3.80	3.98	49.81	46.60
VSM	160	0.99	1.73	82.64	79.17	50	3.60	3.73	38.53	62.89
	20	1.10	1.06	10.92	12.53	60	3.46	3.58	51.49	77.84
	40	1.27	0.53	17.97	17.41	80	3.17	3.27	136.01	135.70
	60	1.15	1.40	37.30	33.21	100	2.91	1.84	197.74	163.50
	80	1.16	0.60	12.69	11.62	10	0.34	0.27	2.02	1.93
	120	0.53	0.56	14.11	11.88	20	0.50	0.42	2.98	2.83
VST	160	0.26	0.23	4.30	2.74	30	0.94	0.66	1.70	2.09
	20	6.65	3.89	14.62	10.98	40	0.92	0.55	1.83	2.11
	40	1.45	1.01	22.14	24.69	50	0.17	0.08	1.12	0.64
	60	1.23	0.85	26.61	25.13	60	0.46	0.18	1.42	1.74
	80	1.05	0.78	29.36	38.78	80	0.81	0.30	2.79	3.22
	120	0.84	0.66	36.70	51.70	100	0.89	0.34	3.16	4.40
	160	0.74	0.55	29.43	27.13	10	4.16	1.73	1.81	1.91
						20	5.01	1.62	2.04	2.15
						30	3.02	0.91	1.83	1.80
						40	4.49	1.41	2.02	1.99
						50	4.26	1.34	1.95	1.97
						60	4.25	1.34	1.90	1.93
						80	3.60	1.14	1.95	1.90
						100	2.98	1.13	1.94	1.96

SMG, semi-arid mountain grassland; DOE, desert–oasis ecotone; PLS, partial least squares regression; SMR, stepwise multiple linear regression; BPANN, back-propagation artificial neural network; NNTS, neural network time series.

Back-propagation artificial network

Back-propagation artificial neural network results for calibration indicated over-fitting, but the performance at SMG was satisfactory (Table 4 and Figure 4). The performance at DOE was worse than at SMG, with the best prediction D_{RP} of soil moisture of 3.16, and that of soil temperature of 2.04; consequently, the performance for DOE was categorized as “B.” A comparison of validation performance for individual soil depths at SMG indicated that both the soil water content and soil temperature results at 20 cm were not as well represented as those at other depths; however, at DOE, there were no noticeable differences among soil depths. The D_{RP} values at DOE ranged from 1.12 to 3.16 for the validation of soil water content, and from 1.81 to 2.04 for the validation of soil temperature.

Neural network time series

We found that the performance of BPANN and NNTS was the same, based on D_{RP} . However, the representation of simulation results at SMG was superior to that at DOE.

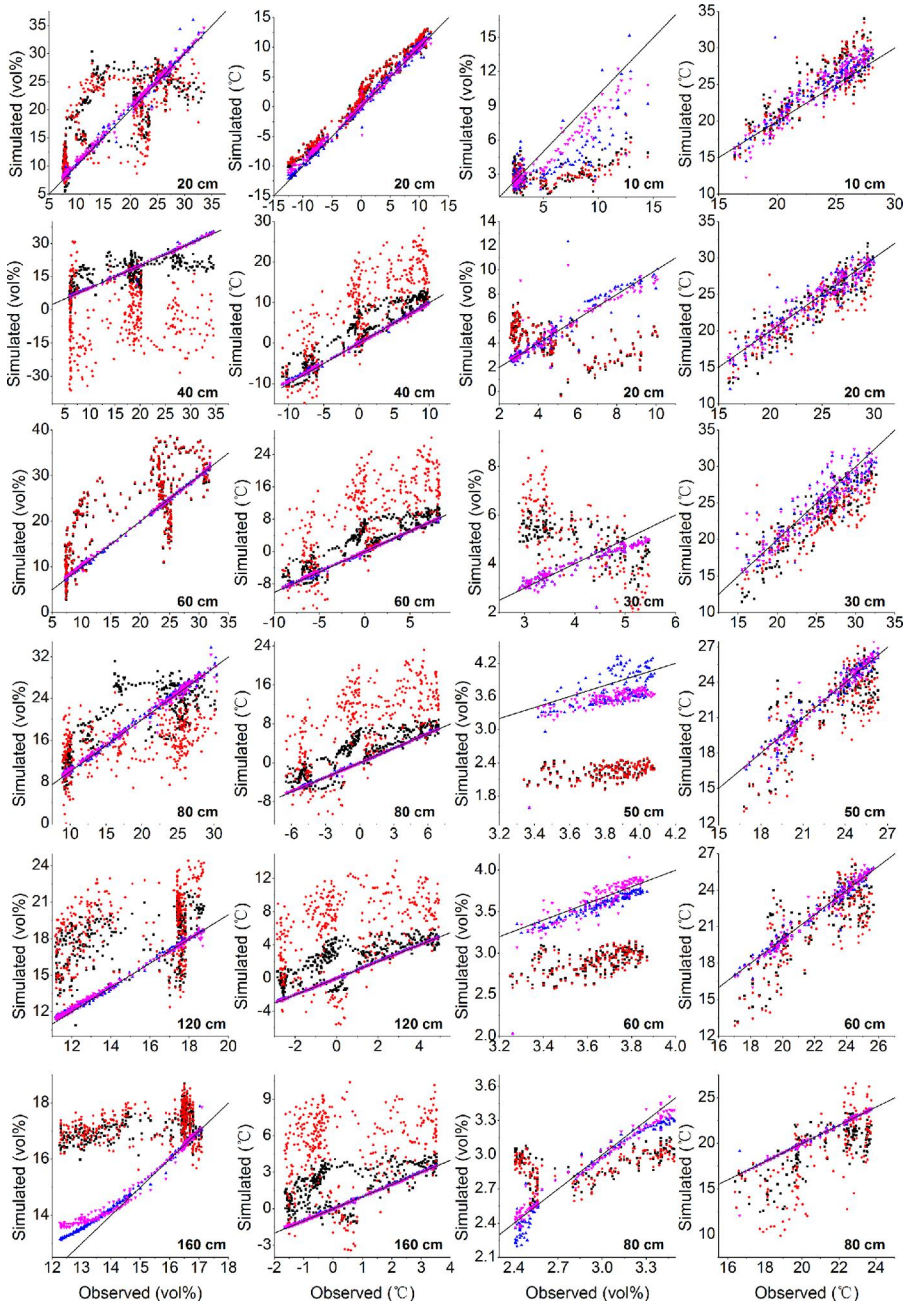


Figure 4. Comparisons of observed vs. Validation data for soil moisture and temperature for individual soil layers obtained with four numerical algorithms: partial least squares regression (black square), stepwise multiple linear regression (red hollow circle), back-propagation artificial neural network (blue upward triangle), and neural network time series (purple downward triangle) at semi-arid mountain grassland (SMG) and desert-oasis ecotone (DOE). In the figure, the first two columns of plots show soil moisture and temperature at SMG. The third and fourth columns show soil moisture and temperature at DOE. Black solid line is the reference line ($y = x$).

The performance at SMG differed across soil depths; optimal results for soil moisture were obtained at 60 cm depth, while those for the surface profile were not satisfactory. Performance at 80–120 cm depth was best for soil temperature validation, and indicated a continuously rising trend with depth of the soil profile.

Discussion

Stability analysis of the models

Grossberg (1988) emphasized that the stability of nonlinear neural networks was one of the characteristics of model validation. Therefore, before model calibration and evaluation, two applications were executed to evaluate the stability of the algorithm.

First, to determine the number of principal components (NPC) of the PLS algorithm in model calibration and validation, we evaluated PLS under different NPCs (from 1 to 7, and 12) (Figure 5). NPC of soil moisture and temperature for the two study sites represented different characteristics in PLS. Soil moisture and temperature forecasting for the surface soil depth needed a larger NPC than that for the subsurface. The NPC in Figure 3 indicates the best results of model evaluation during calibration and validation; in most cases, the NPC differed between the calibration and validation in PLS. Therefore, using the optimal parameters obtained during model calibration may result in suboptimal validation, and model construction may not be optimal either (Grossberg 1988).

Second, we evaluated the performance of the four algorithms for three superficial soil depths after 20 repetitions (Figure 6). Graphical representations (Figure 6) indicated stability of the models used, and the linear algorithms had no uncertainty in the iterations. Contrary to that, the ANNs (BPANN and/or NNTS) were unstable in the iterations due

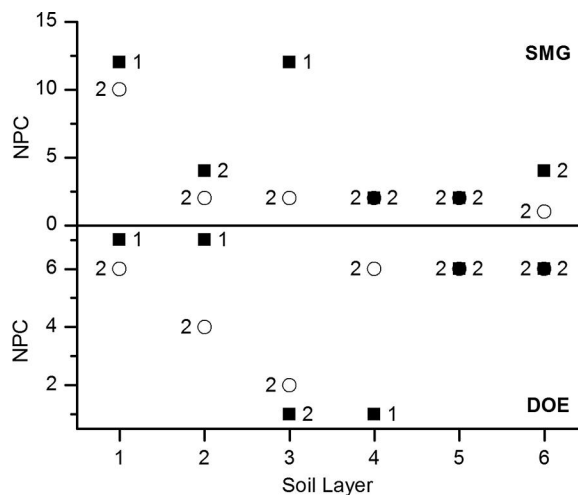


Figure 5. Number of principal components (NPC) of the partial least squares regression (PLS) algorithm between the calibration and validation at different soil layers at two study sites. Shown are soil moisture (black squares) and soil temperature (circles). Label “1” denotes that the NPC remains at the same value between calibration and validation; label “2” means that different labels for soil temperature are found on the left of symbols; labels for soil moisture are found on the right of symbols. DOE: desert–oasis ecotone; SMG: semi-arid mountain grassland. *Note:* Depth of the soil layer was 10, 20, 30, 50, 60, and 80 cm at DOE, and 20, 40, 60, 80, 120, and 160 cm at SMG.

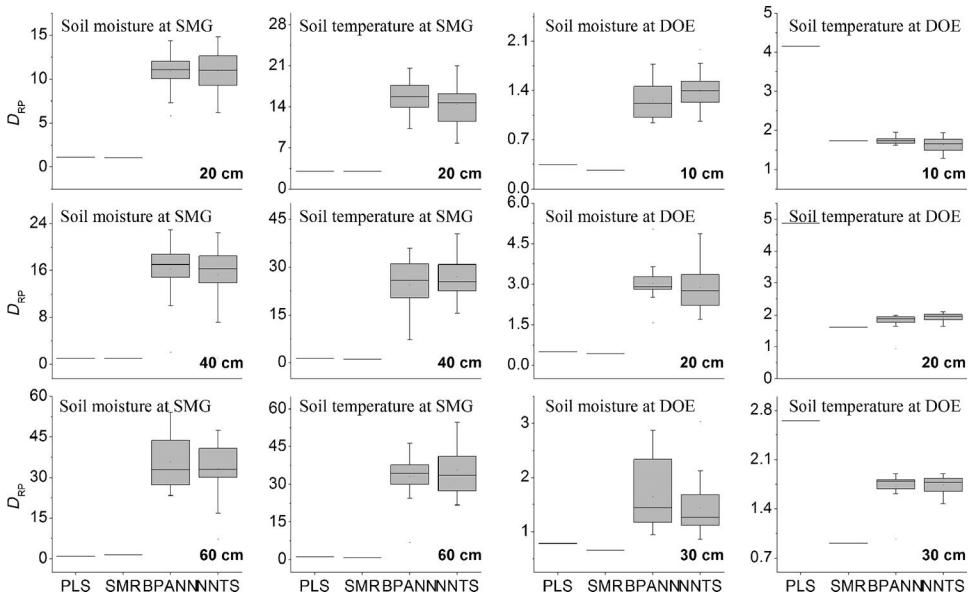


Figure 6. Box-plots showing the stability of the ratio of standard deviation to error sum of squares (D_{RP}) during 20 iterations of validation modeling for the top three soil layers (20, 40, and 60 cm depth at SMG, and 10, 20, and 30 cm depth at DOE) for soil moisture and temperature using four algorithms (PLS, SMR, BPANN, and NNTS). Note: DOE, desert–oasis ecotone; SMG, semi-arid mountain grassland; PLS, partial least squares regression; SMR, stepwise multiple linear regression; BPANN, back-propagation artificial neural network; NNTS, neural network time series.

to the self-learning mechanisms in which learning weights change in every modeling cycle (Dursun and Ozden 2014). Flexibility in the learning weights is one of the advantages of ANNs, but it is also a shortcoming in terms of its stability. Neural networks have a built-in capability to adapt their synaptic weights to changes in the weather environment. However, this adaptability does not always translate into increased robustness (Haykin 1999). This problem was described as the stability–plasticity dilemma (Grossberg 1988; Yu et al. 2012), and further developments need to target the ability to retain the quality of the forecast and to increase the stability of the algorithm.

Precipitation is the critical factor in soil moisture forecasting; however, while the influence of precipitation on soil moisture may be straightforward, the soil moisture–precipitation feedback is complex and affects many processes in the land–atmosphere interactions (Liu et al. 2014; Liu, Mishra, and Yu 2016). Precipitation patterns in arid regions were dominated by small events (≤ 5 mm) although soil moisture was heavily dependent on precipitation (Zhao and Liu 2010). Almost all small rainfall events were consumed by evaporation (radiation forcing) from the land surface (Wei, Dirmeyer, and Guo 2008), and only large or extreme events exerted a strong relationship between soil moisture and rainfall (He et al. 2012). Thus, using climate factors to forecast soil moisture dynamics in arid regions is challenging because only large precipitation events yield a strong connection between the two variables; this was one of the main reasons for an unsatisfactory performance at DOE. The results indicated that climate patterns determined the estimation performance of the algorithms, and that the performance of soil

temperature as a determinant of soil moisture was unsatisfactory. It appears that soil texture is another essential factor that affects heat transfer. High heat conduction, low heat capacity (Hamdhan and Clarke 2010), and high reflectivity of sand may intensify the exchange processes of soil moisture and heat, weakening the relationship between climatic factors, soil moisture, and soil temperature, especially in data-driven modeling. This indicates that arid environments with rapidly evaporating sandy soils and high-frequency small precipitation events need to receive special attention in hydrological modeling.

Box-plots (Figure 6) indicated stability of soil moisture and temperature simulations in shallow soils at SMG and DOE; the interquartile range indicated that soil temperature at SMG had more complex nonlinear relationships with meteorological factors than did soil temperature at DOE. The highest estimation accuracy of PLS was another evidence of these relationships. The results for soil temperature at DOE represented a smaller degree of freedom with D_{RP} than that at SMG, and this suggested that the relationship between climatic factors and soil heat processes was simpler than that for soil moisture. These results indicated that, in synchronized simulations of soil water content and temperature, soil temperature can be calibrated first, and soil water content next; this knowledge will be invaluable for modeling of hydrological processes in rain-fed agriculture in arid areas.

Evaluation of the models

To demonstrate the performance of the four models, we plotted validation results for several soil depths (20, 40, 60, 80, 120, 140, and 160 cm depth at SMG, and 10, 20, 30, 50, 60, and 80 cm depth at DOE) (Figure 4). To obtain a one-to-one correspondence of soil depths, we excluded the 40 and the 100 cm soil layers at DOE. This empirical study showed that, with climatic parameters as the input data, the numerical algorithms were one of the critical steps in the characterization of soil water content and heat at various depths. These results were similar to those in previous studies (Bilgili 2010; Deng et al. 2011). Our study resulted in a new method that increases the understanding of soil water and temperature dynamics especially for regions with dramatically heterogeneous environments.

Clearly, the performances of BPANN and NNTS were superior to those of the other two models, and both PLS and SMR failed to capture the dynamics of most of the processes. These results indicated that the linear statistical forecast models were unable to capture the non-stationary and nonlinear procedures, reflecting the conclusions of Elshorbagy and Parasuraman (2008), and Bilgili (2010). This was evidence of the nonlinear dependency between soil water, soil heat, meteorological factors, and the multilayer perceptron (in machine learning, the perceptron is a function that can decide whether input, represented by a vector of numbers, belongs to some specific class or not). This may be attributed to the fact that a combination of meteorological factors drove the fluctuations in soil water content and heat.

In sharp contrast to SMG, neither BPANN nor NNTS produced ideal results at DOE. Soil water and heating processes and climatic factors generated a weak correlation, especially in the upper soil depths from 10 to 50 cm. A possible explanation may be an interaction of size and frequency of rainfall; namely, rainfall at DOE was frequent and small, or infrequent and extreme (Zhao and Liu 2010), with the majority (82% of total) of events with rain amounts of <5 mm. This configuration indicated that two distinct

rainfall patterns occurred at DOE, which could not be simulated by a single model. Furthermore, during a drought period at DOE, and in general in arid regions, nocturnal “hydraulic lift” by deep-rooted plants may disrupt soil water dynamics and heat distribution in the upper, drier, soil depths (Dawson 1993; Horton and Hart 1998). To obtain a superior simulation performance, rainfall exhibiting two distinct patterns may need to be separated into types, and the types may need separate simulations; further, including the process of hydraulic lift as an input variable at DOE is likely to optimize simulation results.

Interestingly, neither of the two best models, BPANN or NNTS, could depict the lowest water content (<14%) of the deepest soil (about 160 cm) at SMG when analyzed at the level of individual depths. This indicated that the ANN (BPANN, NNTS) could not accurately track the delayed reaction of the deep soil to a long-term drought, a phenomenon observed in this study as well as in previous literature (Elshorbagy and Parasuraman 2008; Latt and Wittenberg 2014). Soil water content at depth may be affected by other processes in addition to climate factors, including the rate of water infiltration, and the presence of bedrock and frozen soil. Water-arrival time in deep soil layers is delayed compared to surface soils, and water is consumed during infiltration. In addition, bedrock or another water-resistant layer can stop the downward movement of soil moisture. For example, frozen soil reallocates heat and concurrently changes both the direction of water movement and the form of water. These factors may affect water-content forecasting in extremely dry conditions (Latt and Wittenberg 2014). These results suggest that studies of soil water content and temperature in arid regions should include measurements of water transfer in the downward as well as upward directions.

The best forecasting of soil moisture in the surface layer at DOE was obtained with $D_{RP} = 2.02$ (BPANN), or the B category, indicating that none of the algorithms can accurately predict soil moisture at 10 cm, and that the response relationships between surface soil moisture and meteorological factors were complex, weak, and nonlinear at DOE; this was similar to the results of soil temperature simulation near the ground surface in Adana City, Turkey (Bilgili 2010). This indicates that in assessments of agricultural irrigation systems in arid areas, soil water content between 20 and 40 cm depth rather than at the surface needs to be used as the quantitative criterion. According to Maheswaran and Khosa (2012), wavelet forms that have variable (compact or wider) subset of the data series can exhibit a better performance in time series, such as short memory with short-duration transient or long-term features. A wavelet is a wave-like oscillation with amplitude that begins and ends at zero.

The results for temperature of surface soil at SMG, for which four algorithms performed well ($D_{RP} \geq 3$, in Table 4), indicated that the response relationship between surface soil temperature (20 cm depth) and meteorological factors can be expressed by a linear function at least to some extent (Bilgili 2010). This was in contrast to soil water content, which for the surface (PLS), and the subsurface (SMR), was represented poorly, and the linear function failed to capture the physical processes in the soil subsurface. In stark contrast to this phenomenon, BPANN and NNTS performed increasingly better with depth of the soil profile, indicating that the algorithm was fully suitable to the specific physical processes. These results suggested that ANNs were preferable for the forecasting of soil heating processes (Gao et al. 2008; Bilgili 2010), and that ANNs can be used as one of the simulation methods for temperate areas, including the oasis–desert transition zones.

Comparing model performance at the two study sites, the D_{RP} in SMG was much higher both for soil moisture and soil temperature than that in DOE. This resulted from vast differences in the range and mean values of soil moisture and temperature at the two sites (Table 1); the mean soil moisture at DOE (3.68%) was far below that at SMG (18.16%), and the range of soil moisture showed the same relative properties (9.55 vs. 32.68%). These results indicated that a strong fluctuation in soil moisture existed at SMG, translating to a powerful response relationship between climatic factors and soil moisture; specifically, the higher the amount of precipitation, the stronger the correlation. This allowed us to capture more easily the changes in soil moisture with meteorological data. The amplitude of soil temperature at SMG (26.08°C) fluctuated less than that at DOE (35.55°C). This suggested that the structure of the system was more complex, and that the ecosystem was more stable at SMG than at DOE. When solar radiation penetrates the atmosphere to the ground surface, it is dissipated in the clouds (via absorption and/or backscatter), by ground vegetation, and by the earth's surface (soils with different moisture contents have different absorption capacities and albedo). Furthermore, more data were available for SMG (680 days) than for DOE (349 days) so that modeling for SMG had sufficient training before model validation; large input datasets are one of the necessary conditions of ANNs for satisfactory forecasting (Haykin 1999; Jain and Kumar 2007).

Conclusion

To improve the performance of soil moisture and heat simulations for different soil depths at two low-moisture sites, SMG and DOE, we evaluated four mathematical algorithms, including BPANN, NNTS, and two linear statistical techniques (PLS and SMR). Evaluation of validation results for soil moisture against known records showed that the best-performing method was BPANN. This indicates that stochastic models can play an important role in estimating hydrological processes, in water resources management and planning, and in the restoration of degraded ecosystems in arid regions.

Semi-arid mountain grassland and DOE had divergent climatic patterns, and algorithm estimation gave two different results; this shows that simulation for two different sites should correspond to the specific climatic patterns. We conclude that forecasting of future soil moisture and/or soil temperature is possible with the use of conventional and easily obtainable meteorological factors without any comprehensive data requirements. This finding is especially valuable in agricultural applications such as irrigation routines and management with limited resources.

To maximize revenue or optimize investing in data sets, data-driven algorithms are the candidate schemes for achieving reliable forecasts in arid regions. Our results revealed that BPANN models forecasted soil water and heat transfer processes well, following a correct training application with meteorological and fractional soil moisture and temperature data (a small subset of data). BPANN can be either linear or nonlinear, and the results can provide useful real-time forecasting and/or irrigation management with limited data resources. Future investigations should be conducted to build more accurate forecasting models for arid regions.

Acknowledgments

We thank the reviewers for their helpful suggestions on this paper. We acknowledge Wei Zhang for the improvements of the original program code.

Funding

This work was supported by funding from the National Science Fund for Excellent Young Scholars (41522102).

References

- Abdi, H. 2007. Partial least square regression (PLS regression). In *Encyclopedia of measurement and statistics*, ed. N. Salkind, pp. 740–744. Thousand Oaks, CA: Sage Publications.
- Ahn, C. 2006. *Advances in evolutionary algorithms: Theory design and practice*. Verlag, Heidelberg, New York: Springer Netherlands, Berlin.
- Bilgili, M. 2010. Prediction of soil temperature using regression and artificial neural network models. *Meteorology and Atmospheric Physics* 110:59–70.
- Breshears, D. D., and F. J. Barnes. 1999. Interrelationships between plant functional types and soil moisture heterogeneity for semiarid landscapes within the grassland/forest continuum: A unified conceptual model. *Landscape Ecology* 14:465–78.
- Brown, M. E., D. J. Lary, A. Vrieling, D. Stathakis, and H. Mussa. 2008. Neural networks as a tool for constructing continuous NDVI time series from AVHRR and MODIS. *International Journal of Remote Sensing* 29:7141–58.
- Chang, C. W., D. A. Laird, M. J. Mausbach, and C. R. Hurburgh. 2001. Near-infrared reflectance spectroscopy-principal components regression analyses of soil properties. *Soil Science Society of America Journal* 65:480–90.
- Dawson, T. E. 1993. Hydraulic lift and water use by plants: Implications for water balance, performance and plant–plant interactions. *Oecologia* 95:565–75.
- Deng, J. Q., X. M. Chen, Z. J. Du, and Y. Zhang. 2011. Soil water simulation and predication using stochastic models based on LS-SVM for red soil region of China. *Water Resources Management* 25:2823–36.
- Dreyfus, G. 2005. *Neural networks methodology and applications*. Paris: Laboratoire d'Electronique, ESPCI.
- Dumedah, G., J. P. Walker, and L. Chik. 2014. Assessing artificial neural networks and statistical methods for infilling missing soil moisture records. *Journal of Hydrology* 515:330–44.
- Dursun, M., and S. Ozden. 2014. An efficient improved photovoltaic irrigation system with artificial neural network based modeling of soil moisture distribution – A case study in Turkey. *Computers and Electronics in Agriculture* 102:120–26.
- Elshorbagy, A., and K. Parasuraman. 2008. On the relevance of using artificial neural networks for estimating soil moisture content. *Journal of Hydrology* 362:1–18.
- Fontaine, J., B. Schirmer, and J. Horr. 2002. Near-infrared reflectance spectroscopy (NIRS) enables the fast; and accurate prediction of essential amino acid contents. 2. Results for wheat, barley, corn, triticale, wheat bran/middlings, rice bran, and sorghum. *Journal of Agricultural and Food Chemistry* 50:3902–11.
- Frank, R. J., N. Davey, and S. P. Hunt. 2001. Time series prediction and neural networks. *Journal of Intelligent and Robotic Systems* 31:91–103.
- Ganguli, P., and M. J. Reddy. 2014. Ensemble prediction of regional droughts using climate inputs and the SVM-copula approach. *Hydrological Processes* 28:4989–5009.
- Gao, Z., R. Horton, L. Wang, H. Liu, and J. Wen. 2008. An improved force-restore method for soil temperature prediction. *European Journal of Soil Science* 59:972–81.
- Grossberg, S. 1988. Nonlinear neural networks: Principles, mechanisms, and architectures. *Neural Networks* 1:17–61.
- Hamdhan, I. N., and B. G. Clarke. 2010. Determination of thermal conductivity of coarse and fine sand soils. Proceedings World Geothermal Congress, Bali, Indonesia, April 25–29.
- Haykin, S. 1999. *Neural networks: A comprehensive foundation*. 2nd ed. Singapore/Delhi: Pearson Education (Singapore) Pte. Ltd., Indian Branch, Delhi, India.

- He, Z. B., X. H. Wen, H. Liu, and J. Du. 2014. A comparative study of artificial neural network, adaptive neuro fuzzy inference system and support vector machine for forecasting river flow in the semiarid mountain region. *Journal of Hydrology* 509:379–86.
- He, Z. B., and W. Z. Zhao. 2004. The spatial heterogeneity of soil moisture in artificial *Haloxylon ammodendron*. *Journal of Glaciology and Geocryology* 26:207–11.
- He, Z. B., W. Z. Zhao, H. Liu, and X. X. Chang. 2012. The response of soil moisture to rainfall event size in subalpine grassland and meadows in a semi-arid mountain range: A case study in northwestern China's Qilian Mountains. *Journal of Hydrology* 420:183–90.
- Horton, J. L., and S. C. Hart. 1998. Hydraulic lift: A potentially important ecosystem process. *Trends in Ecology & Evolution* 13:232–35.
- Hutchinson, C. F., and S. M. Herrmann. 2008. *The future of arid lands-revisited: A review of 50 years of drylands research*. Paris/The Netherlands: UNESCO/Springer.
- Jain, A., and A. M. Kumar. 2007. Hybrid neural network models for hydrologic time series forecasting. *Applied Soft Computing* 7:585–92.
- Klemas, V., C. W. Finkl, and N. Kabbara. 2014. Remote sensing of soil moisture: An overview in relation to coastal soils. *Journal of Coastal Research* 30:685–96.
- Kokaly, R. F., and R. N. Clark. 1999. Spectroscopic determination of leaf biochemistry using band-depth analysis of absorption features and stepwise multiple linear regression. *Remote Sensing of Environment* 67:267–87.
- Koza, J. 1992. *Genetic programming: On the programming of computers by means of natural Selection*. Cambridge, Massachusetts, London, England: The MIT Press.
- Latt, Z. Z., and H. Wittenberg. 2014. Improving flood forecasting in a developing country: A comparative study of stepwise multiple linear regression and artificial neural network. *Water Resources Management* 28:2109–28.
- Liu, D., A. K. Mishra, and Z. B. Yu. 2016. Evaluating uncertainties in multi-layer soil moisture estimation with support vector machines and ensemble Kalman filtering. *Journal of Hydrology* 538:243–55.
- Liu, D., G. L. Wang, R. Mei, Z. B. Yu, and H. H. Gu. 2014. Diagnosing the strength of land-atmosphere coupling at subseasonal to seasonal time scales in Asia. *Journal of Hydrometeorology* 15:320–39.
- Ma, K. M., B. J. Fu, S. L. Liu, W. B. Guan, G. H. Liu, Y. H. Lu, and M. Anand. 2004. Multiple-scale soil moisture distribution and its implications for ecosystem restoration in an arid river valley, China. *Land Degradation & Development* 15:75–85.
- Maheswaran, R., and R. Khosa. 2012. Comparative study of different wavelets for hydrologic forecasting. *Computers & Geosciences* 46:284–95.
- Mevik, B., and R. Wehrens. 2007. The PLS package: Principal component and partial least squares regression in R. *Journal of Statistical Software* 18:1–23.
- Nourani, V., A. H. Baghanam, J. Adamowski, and O. Kisi. 2014. Applications of hybrid wavelet-artificial intelligence models in hydrology: A review. *Journal of Hydrology* 514:358–77.
- Rumelhart, D. E., G. E. Hinton, and R. J. Williams. 1986. Learning representations by back-propagating errors. *Nature* 323:533–36.
- Si, J. H., Q. Feng, X. H. Wen, H. Y. Xi, T. F. Yu, W. Li, and C. Y. Zhao. 2015. Modeling soil water content in extreme arid area using an adaptive neuro-fuzzy inference system. *Journal of Hydrology* 527:679–87.
- Thomas, S., D. H. Qin, and P. Gian-Kasper. 2013. Climate change 2013: The physical science basis. Working group I contribution to the IPCC 5th assessment report – Changes to the underlying scientific/technical assessment. Cambridge University Press, Cambridge.
- Wei, J. F., P. A. Dirmeyer, and Z. C. Guo. 2008. Sensitivities of soil wetness simulation to uncertainties in precipitation and radiation. *Geophysical Research Letters* 35:1–5.
- Wofsy, S. C., M. L. Goulden, J. W. Munger, S. M. Fan, P. S. Bakwin, B. C. Daube, S. L. Bassow, and F. A. Bazzaz. 1993. Net exchange of CO₂ in a midlatitude forest. *Science* 260:1314–17.
- Yang, J. J., Z. B. He, W. J. Zhao, J. Du, L. F. Chen, and X. Zhu. 2016. Assessing artificial neural networks coupled with wavelet analysis for multi-layer soil moisture dynamics prediction. *Sciences in Cold and Arid Regions* 8:0116–24.

- Yilmaz, T., A. Ozbek, A. Yilmaz, and O. Buyukalaca. 2009. Influence of upper layer properties on the ground temperature distribution. *Isi Bilimi Ve Teknigi Dergisi – Journal of Thermal Science and Technology* 29:43–51.
- Yu, Z. B., D. Liu, H. S. Lu, X. L. Fu, L. Xiang, and Y. H. Zhu. 2012. A multi-layer soil moisture data assimilation using support vector machines and ensemble particle filter. *Journal of Hydrology* 475:53–64.
- Zhao, W. Z., and B. Liu. 2010. The response of sap flow in shrubs to rainfall pulses in the desert region of China. *Agricultural and Forest Meteorology* 150:1297–306.
- Zhao, W. Z., Q. Y. Li, and H. Y. Fang. 2007. Effects of sand burial disturbance on seedling growth of *Nitraria sphaerocarpa*. *Plant and Soil* 295:95–102.